Electronic Excitation of $Rh^I(CO)_2$ Species on Al_2O_3 Surfaces: Photodissociation of the Rh^I-CO Bond

Edward A. Wovchko, Tykhon S. Zubkov, and John T. Yates, Jr.*

Surface Science Center, Department of Chemistry, University of Pittsburgh, Pittsburgh, Pennsylvania 15260

Received: July 16, 1998; In Final Form: October 12, 1998

The photoexcitation of $Rh^I(CO)_2/Al_2O_3$ has been studied by infrared and ultraviolet absorption spectroscopy. A photodissociation energy threshold between 2.8 and 2.9 eV, for the Rh^I-CO bond of the $Rh^I(CO)_2$ species, has been determined by monitoring the depletion of the CO moiety, leading to the production of a highly active surface site. A Rh^I-CO photodissociation cross section of 3.6×10^{-20} cm^2 photon^{-1} and a quantum efficiency of 0.01 [Rh^I-CO dissociation] photon^{-1} has been estimated for the initial stages of $Rh^I(CO)_2$ photodepletion. Three absorption bands, observed at 3.3, 3.9, and 4.6 eV in the ultraviolet absorption spectra, are assigned to electronic transitions from filled Rh d-character molecular orbitals to d-character and/or ligand-based antibonding orbitals. Photodissociation of the Rh^I-CO bond occurs from the direct excitation of Rh^I-$(CO)_2$ species. During later stages of photolysis, the role of depletion of $Rh^I(CO)_2$ decreases dramatically and this effect may be due to the slow diffusion of CO through the pores of the Al_2O_3 support.

Introduction

The ultraviolet photolysis of $Rh^I(CO)_2$ supported on an Al_2O_3 surface (designated $Rh^I(CO)_2/Al_2O_3$) results in the loss of a CO ligand and the production of a coordinatively unsaturated Rh^I-(CO) surface species. The coordinatively unsaturated surface site produced is capable of activating strong chemical bonds in molecules which adsorb on these sites. This photochemically generated Rh^I center adsorbs dinitrogen[1], breaks the C−H bond in alkanes,[2−5] breaks the H−H bond in hydrogen,[6] breaks the O=O bond in oxygen,[7] and breaks the C=O bond in CO_2[8] at temperatures below 250 K. However, the exact nature of the photoexcitation responsible for Rh^I-CO bond dissociation leading to the production of the active $Rh^I(CO)/Al_2O_3$ sites has not been investigated. In this paper, we examine in detail the electronic excitation of the Al_2O_3-supported $Rh^I(CO)_2$ species using infrared and ultraviolet absorption spectroscopy.

The photoexcitation of transition metal carbonyl complexes has been a topic of intense research during the past 25 years.[9−13] A recent surge of interest arose from the discovery that some transition metal carbonyls are able to activate C−H bonds in alkanes during ultraviolet irradiation. Hoyano and Graham[14] were the first to report the activation of the C−H bonds in alkanes by a photochemically activated transition metal carbonyl in the early 1980s. Irradiation of $Cp*Ir(CO)_2$ [$Cp* = \eta^5$-C_5-$(CH_3)_5$] with ultraviolet light, creates a coordinatively unsaturated monocarbonyl intermediate by loss of a CO ligand. In an alkane solution, such as C_6H_{12} or $C(CH_3)_4$, oxidative addition of the alkane to this active $Cp*Ir(CO)$ species occurs, generating a stable alkyl hydride organometallic complex. Since that initial study, many have investigated bond activation chemistry during the ultraviolet excitation of various Rh-based transition metal carbonyls, particularly the $CpRh(CO)_2$ and $Cp*Rh(CO)_2$ complexes.[15−22]

The loss of a CO ligand from the ultraviolet photolysis of the $CpRh(CO)_2$ complex has been attributed to the excitation of electrons between the rhodium center d-based orbitals, known as ligand-field (LF) excitations.[9−13] An electron undergoes a vertical transition from a populated metal-centered d-character molecular orbital into the lowest unoccupied molecular orbital (LUMO) that also has significant metal d-character and is antibonding with respect to the ligand. Lees and co-workers[21] have studied ligand substitution (CO/C−H or CO/Si−H) during the laser photolysis of $CpRh(CO)_2$ at 2.7 and 4.0 eV photon energies, where C−H or Si−H bonds were cleaved on the photoproduced Rh site from which a CO ligand had been eliminated. They found that two LF excited states (at 2.9 and 4.3 eV) were involved in the reaction mechanism. The photoexcitation of an electron to the higher lying LF state resulted in facile Rh−CO dissociation, while excitation into the lower LF state was much less efficient and was attributed to a change in Rh−Cp coordination from η^5 to η^3.

We have recently reported ultraviolet−visible absorption spectral measurements of the $Rh^I(CO)_2/Al_2O_3$ species.[23] The electronic transitions observed in the spectra for the surface Rh^I-$(CO)_2/Al_2O_3$ species closely corresponded to the electronic spectrum of various homogeneous phase $[Rh^IX_2(CO)_2]^-$ (X = Cl, Br) anions[24,25] and of the chloro-bridged $[Rh^ICl(CO)_2]_2$ complex.[25] The close similarity between the UV−Vis spectrum of the $Rh^I(CO)_2$ species in homogeneous phase and the surface analogue, demonstrated unequivocally that the Rh^I ion is produced during the chemisorption of CO on Rh/Al_2O_3 catalysts.[23] The molecular orbital energy diagram describing the Rh^I-$Cl_2(CO)_2$ moiety in the $[Rh^ICl(CO)_2]_2$ complex was used to explain the electronic transitions observed in the ultraviolet absorption spectrum of the $Rh^I(CO)_2/Al_2O_3$ surface species.

By spectroscopically monitoring the time-dependent photodecomposition of $Rh^I(CO)_2$ during irradiation at various photon energies, we have determined the Rh^I-CO bond photodissociation energy threshold. The onset of Rh^I-CO photodissociation corresponds to observed electronic excitations within the $Rh^I(CO)_2/Al_2O_3$ species.

2. Experimental Section

2.1. Infrared Experiments. The transmission infrared spectroscopic experiments were conducted in the special cell adopted to combine FTIR and simultaneous UV excitation, as described in detail previously.[26,27] The cell is a stainless steel cube with six conflat flange ports. Two CaF_2 windows, sealed with differentially pumped double O-rings were used on two ports for infrared beam transmission. A third differentially pumped CaF_2 window was used to admit ultraviolet radiation. Samples were spray-deposited on a tungsten support grid (0.0254 mm thick with 0.22 mm square openings exhibiting 70% optical transparency). Both IR and UV radiation are incident at a 45° angle to the plane of the grid support.[27] The grid was secured by nickel clamps and mounted on electrical feedthroughs connected to the bottom of a reentrant Dewar which enters the cell. The grid and sample could be heated electrically using a digital temperature programmer/controller.[28] Sample cooling was achieved by filling the reentrant Dewar with liquid nitrogen. A K-type thermocouple spot welded on the top center of the tungsten grid measured sample temperatures. The temperature could be held constant and maintained to ±2 K in the range 140−1500 K. The cell was connected via stainless steel bellows tubing to a bakeable stainless steel vacuum and gas delivery system. The system was pumped by 60 L s^{-1} turbomolecular and 30 L s^{-1} ion pumps, achieving base pressures <1 × 10^{-7} Torr. The system was equipped with a Dycor M100M quadrupole mass spectrometer for gas analysis and leak checking. Gas pressures were measured with a MKS 116A Baratron capacitance manometer.

The 0.5% Rh/Al_2O_3 samples were prepared by dissolving $RhCl_3 \cdot 3H_2O$ (Alfa 99.9%) in ultrapure H_2O (10 mL/g of support). The solution was mixed with the appropriate amount of powdered Al_2O_3 (Degussa, 101 m^2/g) and ultrasonically dispersed for approximately 45 min. This slurry was then mixed with acetone (Mallinckrodt, AR) (9:1-acetone/H_2O volume ratio) and sprayed onto the tungsten grid using a nitrogen-gas pressured atomizer. The grid was warmed (~330 K), and spraying was interrupted intermittently to allow for solvent evaporation. The mixture was sprayed on a 2:3 section (3.0 cm^2) of the grid leaving a shielded 1:3 (1.5 cm^2) section clear for background scans. A single 34 mg (11.3 mg/cm^2) sample was reused for each infrared experiment.

Immediately after spraying, the sample was transferred to the infrared cell and evacuated at 475 K for 14 h. Following evacuation, the sample was reduced at 475 K using three 175 Torr H_2 exposures of 15 min each, and one 200 Torr H_2 exposure of 60 min duration, with evacuation after each exposure. The sample was evacuated at 475 K for another 2 h then cooled to 303 K and exposed to 10 Torr of CO for 10 min to convert the metallic Rh to $Rh^I(CO)_2$. The cell was evacuated, and the sample was cooled to 205 K prior to each photolysis experiments. After each experiment, the sample was warmed to 303 K and reexposed to 10 Torr of CO for 10 min, followed by evacuation and cooling. The initial small increase in sample temperature due to irradiation was compensated by the temperature controller.

Infrared spectra were measured using a nitrogen-gas purged Mattson Research Series I Fourier transform infrared spectrometer equipped with a liquid nitrogen cooled HgCdTe wide band detector. Infrared spectra were recorded at various intervals after periods of photolysis using a self-designed data acquisition program. During initial stages of photolysis (3−900 s), 36 scans were averaged, requiring ~8 s per spectrum. For later stages of photolysis (900−1.8 × 10^4 s), 100 scans were averaged,

requiring ~23 s per spectrum. A spectral resolution of 4 cm^{-1} and a signal gain of 4 were employed for each measurement. Prior to photolysis experiments, the cell was translated laterally so the beam could pass through the unsprayed portion of the grid to obtain the background spectrum. Small background features due to small deposits on the KBr windows were observed. Absorbance spectra of the sample were obtained by ratioing single beam spectra of the sample to background single beam spectra. Spectra were then automatically baseline corrected and normalized.

A 350 W high-pressure mercury arc lamp provided both ultraviolet and visible light for photolysis experiments. The optical bench was equipped with a *f*/1 two element UV fused silica condensing lens, an iris diaphragm, and a shutter. The light was filtered by a 10 cm water infrared radiation filter and then by one of a variety of band-pass/cutoff filters with an average energy in the range of 2.8 to 3.9 eV. Photon fluxes in the UV region (responsible for Rh^I−CO dissociation) ranged from 8.5 × 10^{16} to 1.4 × 10^{17} photons cm^{-2} s^{-1} depending upon the filter. Photochemistry and infrared measurements were conducted simultaneously without disturbing the position of the cell or UV lamp.

2.2. Ultraviolet Absorption Experiment. A cell, similar to the one used by Beebe et al. and others[29,30] for measuring infrared spectra of powdered samples, was used to measure the ultraviolet spectrum of $Rh^I(CO)_2/Al_2O_3$. The cell consists of a copper support ring which rigidly holds a 2.5 cm diameter highly polished CaF_2 disk on which the powdered sample is deposited. A K-type thermocouple is connected to the Cu ring. The thermocouple wires are spot-welded to the leads of K-type thermocouple feedthrough that is welded to the cell body. A port drilled into the cell body is connected to a stainless steel valve which is used to connect the cell to the vacuum system. The cell contains two commercially obtained CaF_2 windows sealed in 2.75" conflat flanges. The sample was heated by wrapping the entire cell body with a heating tape and applying AC power to the heating tape. The temperature of the heating tape, and thus the sample, was controlled by a Micromega CN7700 Series programmable PID temperature controller connected in series to a variable transformer. Constant sample temperatures could be maintained at ±1 K.

A vacuum/gas delivery system, similar to that used in the infrared measurements, was constructed for the sample treatment and gas exposure.

A Perkin-Elmer Model Lambda 9 double beam, grating ultraviolet−visible spectrophotometer was employed. A specially designed cell mounting bracket was machined to fit the sample compartment of the spectrometer. The bracket permitted both vertical and lateral translation of the cell and was able to maintain a rigidly fixed cell position during the course of spectroscopic measurements. Due to the high scattering of UV light from the small particle size of the deposited Al_2O_3 nanoparticles (13 nm average particle size), the intensity of transmitted light was very low making spectroscopic measurements difficult. To overcome this problem, a slit width of 5 nm was used to maximize the incident light intensity. Also, 10 spectral scans were accumulated and signal averaged to increase the signal-to-noise ratio.

The 0.5% Rh/Al_2O_3 sample was prepared as indicated above. The slurry was sprayed onto a one-half portion of the warmed (~330 K) CaF_2 disk, leaving the other half portion clear for background scans. A low sample density of 1.2 mg/cm^2 was deposited onto the disk to reduce the extent of scattering of the UV radiation.
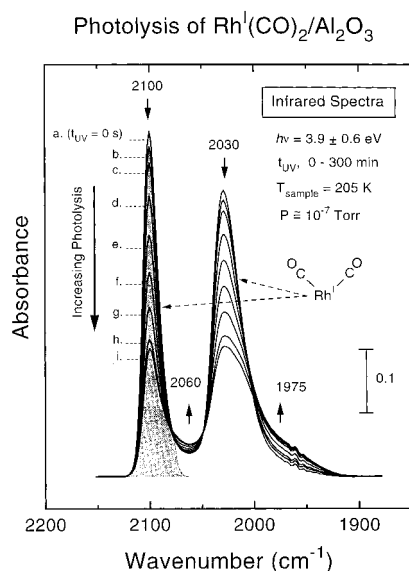
Excitation of Rh^I(CO)$_2$ Species on Al$_2$O$_3$ Surfaces

J. Phys. Chem. B, Vol. 102, No. 51, 1998 **10537**

Figure 1. Selected infrared spectra measured in the C−O and stretching region during 1.8×10^4 s (300 min) of 3.9 ± 0.6 eV ultraviolet photolysis of Rh^I(CO)$_2$/Al$_2$O$_3$ at 205 K under evacuation. The arrows indicate the direction of the absorbance changes. The photolysis time for each spectrum is as follows: (a) 0 s, (b) 3 s, (c) 30 s, (d) 240 s, (e) 810 s, (f) 2100 s, (g) 4800 s, (h) 10800 s, (i) 18000 s. (Note: Spectra have been base line corrected.)

Figure 2. The normalized absorbance loss of the 2100 cm^{-1} ν_{sym}-(CO) mode of Rh^I(CO)$_2$ species as a function of photolysis time at various photon energies. Each loss curve has been fit to a double-exponential decay for each energy greater than 2.8 eV, as shown by the white line.

After spraying, the disk containing the sample was transferred to the cell and evacuated at 475 K for 10 h. Following evacuation the sample was reduced as described above. A saturation exposure for $\sim$ 12 h at 30 Torr CO was used, followed by evacuation for 15 min prior to spectral measurements. Thus, the preparation of the Rh^I(CO)$_2$/Al$_2$O$_3$ samples for both UV and IR measurements was essentially identical.

For both the UV and IR experiments, carbon monoxide (Airco 99.999%) was obtained in an aluminum cylinder and transferred to a previously evacuated and baked glass bulb and used without further purification. Hydrogen (Matheson, 99.9995%) was obtained in a steel cylinder and was also used without further purification.

3. Results

3.1. Photolysis of Rh^I(CO)$_2$/Al$_2$O$_3$ in Vacuum. Figure 1 shows selected infrared spectra measured during 1.8×10^4 s ultraviolet photolysis of Rh^I(CO)$_2$ supported on Al$_2$O$_3$ at 205 K while under evacuation ($\sim$10^{-7} Torr). The initial spectrum measured prior to any UV irradiation (spectrum a: $t_{UV} = 0$ s) displays two strong infrared bands at 2100 and 2030 cm^{-1}. These bands occur in the C−O region for the symmetric and antisymmetric stretching modes of Rh^I(CO)$_2$ (rhodium gem-dicarbonyl).[30−41] The isolated Rh^I(CO)$_2$ species are formed from the disruption of metallic Rh in a reaction with CO and hydroxyl groups (Al−OH) on the Al$_2$O$_3$ support.[38−41] It is noted that, initially, there is very little contribution to the infrared spectrum near 2060 and 1850 cm^{-1} (1850 cm^{-1} region not shown), indicating that only a small fraction of rhodium exists as metallic Rh. Rhodium centers forming Rh^I(CO)$_2$ are highly dispersed over the support.

Immediately after opening the Hg arc lamp shutter, the absorbance of the two bands at 2100 and 2030 cm^{-1} decreases (the direction of absorbance change is shown by the arrows) indicating the photochemical destruction of Rh^I(CO)$_2$ species as Rh^I−CO bonds are cleaved and CO ligands are lost. Infrared spectra were continually measured following $3-1.8 \times 10^4$ s of
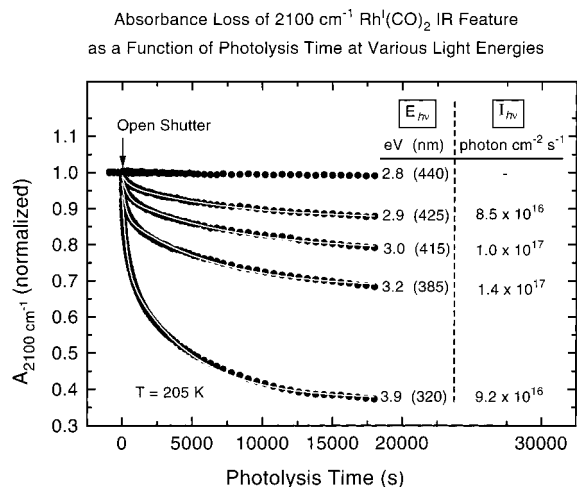
ultraviolet photolysis. The depletion is accompanied by the development of two weak infrared features near 2060 and 1975 cm^{-1}. These two features overlap the wings of the antisymmetric C−O stretching mode of the Rh^I(CO)$_2$ species at 2030 cm^{-1}. The depleting 2030 cm^{-1} band masks the development of these two bands as indicated by the change in the relative absorbance ratio of the symmetric and antisymmetric stretching modes of the Rh^I(CO)$_2$ species. These two features have been assigned to the coordinatively unsaturated Rh^I(CO) and Rh$^I_2$(CO)$_2$ species, respectively.[1]

3.2. Rh^I(CO)$_2$ Depletion as a Function of Photolysis Energy. The rate of loss of the 2100 cm^{-1} infrared feature has been examined during irradiation at various photon energies, as shown in Figure 2. The normalized absorbance of the 2100 cm^{-1} feature has been plotted as a function of photolysis time for five different average energies from 2.8 to 3.9 eV, provided by the filtered Hg arc lamp. Also included in Figure 2 is the photon flux $I_{h\nu}$ for each energy. For photon energies up to 2.8 eV, no loss of the 2100 cm^{-1} Rh^I(CO)$_2$ infrared feature takes place. One may observe that the rate and extent of Rh^I(CO)$_2$ depletion increases as the sample is exposed to higher photon energies. The curves for energies greater than 2.8 eV have been fit, as shown by the white lines, using a double exponential rate law. The use of these fits, to determine the Rh^I−CO photodissociation threshold energy and cross section, will be described later in the Discussion section.

3.3. Ultraviolet Absorption Spectra of Rh^I(CO)$_2$/Al$_2$O$_3$. The ultraviolet absorption spectra measured during the chemisorption of CO on 0.5% Rh/Al$_2$O$_3$ are shown in Figure 3A. Three absorption features develop at 3.3, 3.9, and 4.6 eV as the exposure to CO(g) increases from $1 \times 10^{-3}-30$ Torr. These absorption features correspond to electronic excitations taking place within Rh^I(CO)$_2$/Al$_2$O$_3$ species which are formed from the disruption of metallic Rh in a reaction with CO and Al−OH groups as discussed above. A more detailed presentation of the ultraviolet spectroscopic measurements and the complementary infrared spectroscopic measurements of the developing Rh^I(CO)$_2$ species with increasing CO exposure, can be found in another publication[23] where a linear correlation was found between the absorbance of the IR and ultraviolet spectra. The predominant infrared features measured following the 30 Torr CO exposure are very similar to these shown in Figure 1, spectrum a, and compare well to the gas-phase frequencies of
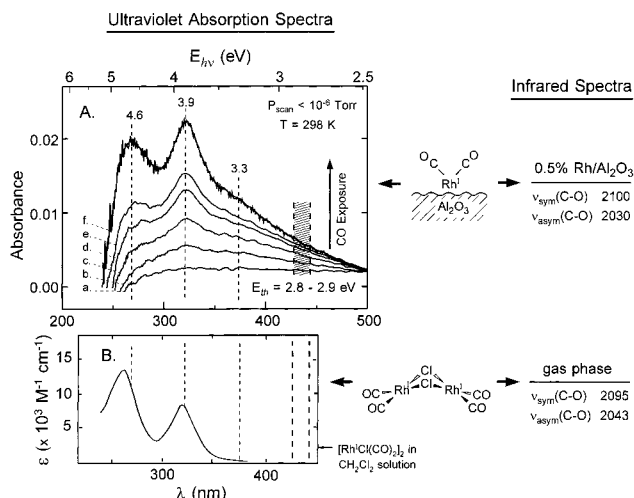
10538 *J. Phys. Chem. B, Vol. 102, No. 51, 1998*

Wovchko et al.

Spectroscopic Comparison of Rh^I(CO)$_2$/Al$_2$O$_3$ to [Rh^{I}Cl(CO)$_2$]$_2$

Figure 3. Spectroscopic Comparison of Rh^I(CO)$_2$/Al$_2$O$_3$ to [Rh^{I}Cl-(CO)$_2$]$_2$. (A) The ultraviolet absorption spectra measured during the chemisorption of CO on 0.5% Rh/Al$_2$O$_3$ at 300 K. CO(g) exposures are as follows: (a) 1 mTorr, (b) 10 mTorr, (c) 100 mTorr, (d) 1 Torr, (e) 10 Torr, (f) 30 Torr. The Rh^I−CO photodissociation threshold energy range is indicated by the shaded region. (Note: The UV spectrum measured prior to CO exposure has been subtracted from each spectrum. A 15-point cubic smoothing function has been applied to each spectrum. Both the original and smoothed spectra are shown for f.) (B) The ultraviolet absorption spectrum measured for [Rh^{I}Cl(CO)$_2$]$_2$ in CH$_2$Cl$_2$ solution. Reproduced from Epstein et al., ref 25. Infrared spectral bands for gas phase [Rh^{I}Cl(CO)$_2$]$_2$ from Garland et al., ref 42.

2095 and 2043 cm^{-1} for the [Rh^{I}Cl(CO)$_2$]$_2$ complex.[42] It is clear that the ultraviolet absorption bands observed in Figure 3A are due to excitations occurring in Rh^I(CO)$_2$ species.

The ultraviolet absorption bands measured in Figure 3A can be compared to the ultraviolet absorption bands measured for the [Rh^{I}Cl(CO)$_2$]$_2$ inorganic complex in a CH$_2$Cl$_2$ solution that have been reproduced in Figure 3B.[25] The two ultraviolet absorption bands at 4.6 and 3.9 eV for Rh^I(CO)$_2$/Al$_2$O$_3$ correlate very well with the two intense absorption bands observed at 4.8 and 3.9 eV for [Rh^{I}Cl(CO)$_2$]$_2$. Although not observed in Figure 3B, the weak absorption band measured at 3.3 eV for supported Rh^I(CO)$_2$ species (Figure 3A) does in fact have a weak counterpart at 3.4 eV in the magnetic circular dichroism (MCD) spectrum of [Rh^{I}Cl(CO)$_2$]$_2$ in CH$_2$Cl$_2$ and other solvents.[25] The close similarity between the ultraviolet absorption spectra for the homogeneous and heterogeneous Rh^I(CO)$_2$ species indicates that comparable electronic excitation processes are taking place.

4. Discussion

4.1. Photochemistry of Rh^I(CO)$_2$/Al$_2$O$_3$−Rh^I−CO Bond Dissociation.
The ultraviolet photolysis of Rh^I(CO)$_2$/Al$_2$O$_3$ results in the excitation of the Rh^I(CO)$_2$ species followed by the loss of a CO ligand and the production of coordinatively unsaturated Rh^I(CO) and CO(g) according to the first-order reaction shown below:

$$Rh^I(CO)_2 + h\nu \rightarrow Rh^I(CO)_2{}^* \rightarrow Rh^I(CO) + CO(g) \quad (1)$$
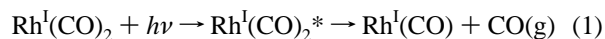
The desorption of CO, as a result of UV irradiation of Rh^I-(CO)$_2$/Al$_2$O$_3$, was first observed with a mass spectrometer and by IR spectroscopy by Ballinger et al.[3]

Here we have studied the photoexcitation of Rh^I(CO)$_2$/Al$_2$O$_3$ in more detail by directly monitoring the loss of the Rh^I(CO)$_2$

infrared bands (Figures 1 and 2) during UV irradiation. By working at 205 K, possible thermal effects were minimized. The photodecomposition of Rh^I(CO)$_2$ species takes place at photon energies greater than 2.8 eV (Figure 2). An energy threshold in this region is typical for transition metal−carbonyl photodissociation processes in homogeneous phase.[9] For example, dissociation of CpRh(CO)$_2$ takes place during ultraviolet excitation between 2.7 and 4.3 eV.[21]

The rate of CO loss from Rh^I(CO)$_2$/Al$_2$O$_3$ species increases during irradiation at higher photon energies (Figure 2). The gain in the rate of Rh^I−CO dissociation as the photon energy is increased, may be explained by two viable processes: (1) excitation into higher lying vibrational levels of a particular energy level for an excited state that can overcome the barrier for dissociation and (2) excitation into higher lying electronic levels that are dissociative in Rh^I−CO.

4.2. Rh^I−CO Photodissociation−Cross Section and Quantum Efficiency Estimations. The probability of a photochemically driven event may be expressed as a cross section, σ (cm^2 photon^{-1}). Assuming first-order kinetics, the cross section for a photodissociative process occurring on a surface can be obtained from the slope of the semilogarithmic plot of the adsorbate coverage versus incident photon fluence.[43] In Figure 2, the depletion of Rh^I(CO)$_2$ during 1.8×10^4 s of ultraviolet irradiation does not follow first-order kinetics.

The photodepletion of Rh^I(CO)$_2$, as measured by the change in IR absorbance, $A_{2100 \text{ cm}^{-1}}$, may be accurately fit using a double exponential rate law expressed as

$$\frac{A}{A_o} = b_1 e^{-k_i I_{h\nu} t} + b_2 e^{-k_d t} + c \quad (2)$$

where k_i is the first-order rate constant for the photodepletion process, $I_{h\nu}$ is the photon flux, t is the irradiation time, and c is a constant that corrects for the nonzero endpoint. The second term in eq 2 involves an empirical constant, k_d, which may be related to a slow CO diffusion process which retards the Rh^I-(CO)$_2$ depletion for the porous Al$_2$O$_3$ powder supporting the Rh^I(CO)$_2$ species. The fits to eq 2 are shown in Figure 2 for each photolysis experiment conducted with photon energies greater than 2.8 eV.

The two kinetic processes, governing the photodepletion of Rh^I(CO)$_2$, can also be distinguished by examining the natural log plot of the normalized absorbance corrected for the nonzero endpoint, $A_{2100 \text{ cm}^{-1}} - c$, as a function of the photolysis time. This is shown for the 3.9 ± 0.6 eV photolysis experiment in Figure 4. The inflection point occurring near 300 s is indicative of the increasing influence of the slow kinetic process on the rate of photodepletion. The rate constant for Rh^I(CO)$_2$ photodepletion k_i is obtained from the slope of the linear fit for the initial stage of photolysis (0−60 s), defining the magnitude of the first exponential term in eq 2. The empirical constant related to the slow CO depletion process is obtained from the linear fit for the later stage of photolysis (450−1.5×10^4 s), and defines the magnitude of the second exponential term in eq 2.

The cross section σ_i for the photodepletion process is determined from the rate constant k_i and the photon flux. The photon flux, provided by the Hg arc lamp, was measured for each filter used in the photodepletion experiments (Figure 2). The average energy, the corresponding photon flux, and the calculated cross section for each experiment are presented in Table 1.

The Rh^I(CO)$_2$ photodepletion cross section is plotted as a function of the average photon energy in Figure 5. This plot shows that the Rh^I−CO photodissociation energy threshold is

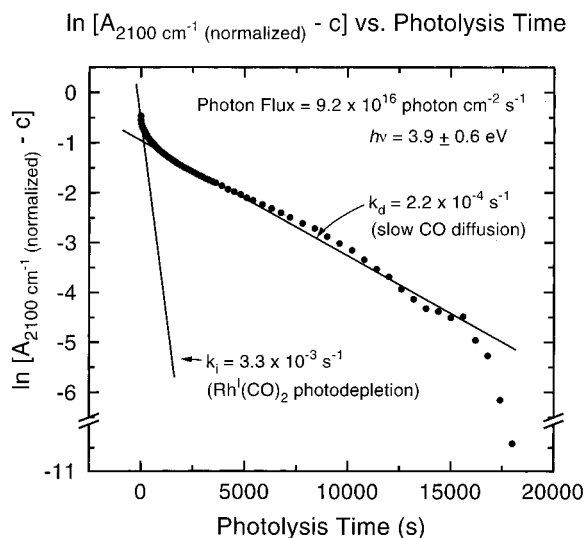Excitation of Rh^I(CO)$_2$ Species on Al$_2$O$_3$ Surfaces

J. Phys. Chem. B, Vol. 102, No. 51, 1998 **10539**

Figure 4. Natural log plot of the Rh^I(CO)$_2$ photodepletion, $A_{2100\,cm^{-1}}$ − c, as a function of photolysis time for $h\nu$ = 3.9 ± 0.6 eV.
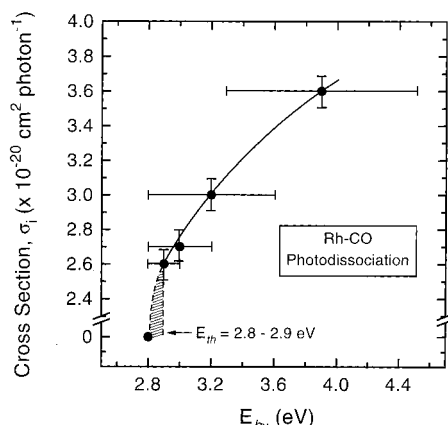
Figure 5. Energy threshold determination for Rh^I−CO photodissociation. The cross section for Rh^I(CO)$_2$ photodepletion is plotted as a function of the average photolysis energy. The horizontal bars show the range of energies for each filter used.

TABLE 1: Photon Flux and Cross Section for Each Photon Energy During Rh^I(CO)$_2$ Photodepletion Experiments

| $E_{h\nu}$ (eV)	k_i (s^{-1})	photon flux $I_{h\nu}$ (photon cm^{-2} s^{-1})	cross section σ_i (cm^2 photon^{-1})
<2.8			0
2.9 ± 0.1	2.2 × 10^{-3}	8.5 (±0.2) × 10^{16}	2.6 (±0.08) × 10^{-20}
3.0 ± 0.2	2.7 × 10^{-3}	1.0 (±0.03) × 10^{17}	2.7 (±0.08) × 10^{-20}
3.2 ± 0.4	4.2 × 10^{-3}	1.4 (±0.03) × 10^{17}	3.0 (±0.08) × 10^{-20}
3.9 ± 0.6	3.3 × 10^{-3}	9.2 (±0.2) × 10^{16}	3.6 (±0.08) × 10^{-20}

between 2.8 and 2.9 eV and that the rate of photodepletion increases for higher photon energies.

The quantum efficiency for Rh^I−CO dissociation can be approximated for the initial stage of photolysis by considering the ratio in eq 3 between the extent of Rh^I(CO)$_2$ loss and the number of photons exposed to the sample.

$$\Phi_i = \frac{\text{Number of Rh}^I(\text{CO})_2 \text{ lost cm}^{-2}\,\text{s}^{-1}}{\text{Number of Photons cm}^{-2}\,\text{s}^{-1}} =$$

$$\frac{[\text{Rh}^I(\text{CO})_2 \text{ species}]\,\text{cm}^{-2}\,k_i}{I_{h\nu}} \quad (3)$$

For a 11.3 mg cm^{-2} deposit of 0.5%Rh/Al$_2$O$_3$, approximately

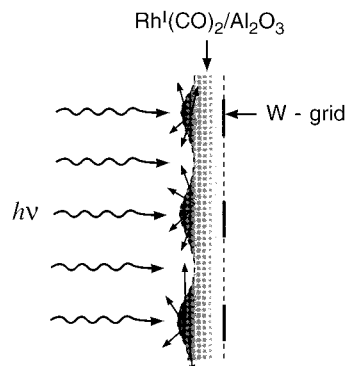## A. Slow CO Diffusion Through Pore
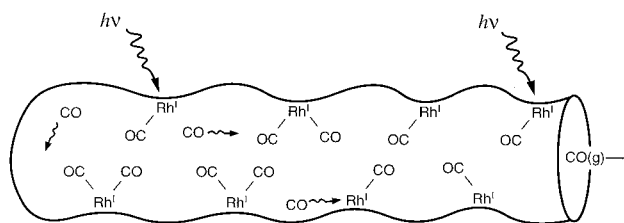
B. Limited Penetration of Light into Sample

Figure 6. Schematic representation of factors affecting Rh^I(CO)$_2$ photodecomposition kinetics. (A) Secondary process involving the slow diffusion of CO through pores of Al$_2$O$_3$ support. Readsorption of CO on Rh^I(CO) sites is believed to be a significant factor limiting the rate of depletion of Rh^I(CO)$_2$ during photolysis. (B) Limited penetration of light into the powdered sample as a result of scattering and reflection. This factor may cause the photodepletion cross section estimates to be lower limits in these experiments.

3.3 × 10^{17} [Rh^I(CO)$_2$ species] cm^{-2} exist, assuming that every Rh site is a gem-dicarbonyl species. At a photon energy of 3.9 ± 0.6 eV, an initial rate constant, k_i, of 3.3 × 10^{-3} s^{-1} and a photon flux, $I_{h\nu}$, of 9.2 × 10^{16} photon cm^{-2} s^{-1} gives a quantum efficiency of approximately 0.01 Rh^I(CO)$_2$ lost per photon.

The value of Φ_i decreases dramatically during photolysis, and complete depletion of Rh^I(CO)$_2$ species is not observed even after 1.8 × 10^4 s (Figures 1 and 2). This decreasing rate of CO loss may be explained by a second rate-controlling process which may involve the slow diffusion of CO in the pores of the Al$_2$O$_3$ support as shown pictorially in Figure 6A. Slow diffusion of CO in pores (either gas phase diffusion and/or surface diffusion) was responsible for the nonequilibrium exchange of isotopically labeled C*O(g) with Al$_2$O$_3$ supported Rh^I(CO)$_2$ species.[36] One can imagine a similar process limiting the rate of Rh^I(CO)$_2$ depletion during ultraviolet photolysis. In addition to slow CO diffusion, readsorption of a CO molecule onto a vacant Rh^I(CO) site may also occur. One may envision cage-type effects where a photodesorbed CO molecule is confined in a small pore and readsorbs onto coordinatively unsaturated Rh sites, unable to escape into vacuum. On this basis, preferential loss of CO from Rh^I(CO)$_2$ species near the exit regions of internal pores in the Al$_2$O$_3$ would be expected, and following this initial depletion process, a dramatic retardation of depletion rate would be expected as photolysis occurs at Rh^I(CO)$_2$ sites deep in the pores. The constant k_d empirically describes this process well. It is also possible that the slow kinetic process is related to the reduction of UV light intensity within the pores of the Al$_2$O$_3$.

The efficiency of Rh[I]−CO photodissociation is also limited by the transmission of UV light through the powdered material. Scattering and reflection of ultraviolet light from Al_2O_3 particles will inhibit the penetration of light into the underlying layers of the deposited powder. This is shown pictorially in Figure 6B. The reduced light intensity in these regions will result in a lower probability for light absorption and subsequent photodesorption of CO, causing estimates of σ_i and Φ_i to be too low.

4.3. Electronic Excitation Processes Leading to Rh[I]−CO Dissociation. The ultraviolet irradiation of $Rh^I(CO)_2$ supported on Al_2O_3 causes direct electronic excitation of the $Rh^I(CO)_2$ species. The excitation involves primarily ligand field and/or metal-to-ligand charge-transfer transitions, much like the transitions involved during the photoexcitation of transition metal carbonyls in homogeneous phase.[9−13] Excitation of electrons from the Al_2O_3 substrate does not influence the Rh[I]−CO photodissociation, since the band gap of Al_2O_3 is ∼5.5 eV. Furthermore, substrate-mediated excitation of supported metallic Rh metal to produce photoelectrons or hot electrons that can potentially participate in Rh−CO dissociation is not likely for two reasons. First, only a small fraction of the supported Rh exists as metallic Rh based on the infrared spectroscopic measurements after CO adsorption (Figure 1), where CO chemisorbed on metallic Rh is hardly observed.[38] Second, the work function of Rh metal is ∼4.75 eV,[44] eliminating the possibly of photoelectron participation. Also, the photoinduced desorption of CO adsorbed on Rh sites of a Rh(100) single crystal was not reported during the ≤4.5 eV ultraviolet irradiation of $Mo(CO)_6$/CO/Rh(100)[45] eliminating the possibility of hot electron participation. The photodecomposition of the adsorbed $Mo(CO)_6$ complex to produce $Mo(CO)_{6−x}$ and CO-$(g)_x$ was reported, however, and the authors attributed the M−CO dissociation to direct excitation of the adsorbed complex.[45]

4.4. Electronic Excitation of $Rh^I(CO)_2$/Al_2O_3. We have recently provided the first direct spectroscopic evidence in the UV region for the formation of $Rh^I(CO)_2$ species when metallic Rh/Al_2O_3 is treated with CO by measuring the ultraviolet absorption spectra.[23] The spectra of $Rh^I(CO)_2$/Al_2O_3 (Figure 3A) show two strong bands centered at 3.9 and 4.6 eV and a weak feature centered near 3.3 eV. The tail of the 3.3 eV feature is located near the 2.8−2.9 eV Rh[I]−CO photodissociation threshold energy (shaded region of Figure 3A), determined from the kinetic measurements during irradiation at different energies (Figure 5). The detection of the two UV absorption bands at 3.9 and 4.6 eV is also consistent with the observed increase in Rh[I]−CO photodissociation during irradiation at higher energies (up to 4.5 eV). Therefore, the observed absorption bands measured in the UV spectra of $Rh^I(CO)_2$/Al_2O_3 are probably indicative of multiple electronic transitions taking place within $Rh^I(CO)_2$ species that result in the Rh[I]−CO bond breaking.

The $Rh^I(CO)_2$/Al_2O_3 species has been spectroscopically compared on numerous occasions to the $[Rh^ICl(CO)_2]_2$ inorganic complex for both geometric and Rh oxidation state purposes.[31−33,36,38,39] In Figure 3 and in ref 23 we have compared the ultraviolet absorption bands of $Rh^I(CO)_2$/Al_2O_3 species to the absorption bands measured by Epstein et al.[25] for $[Rh^ICl$-$(CO)_2]_2$ in CH_2Cl_2 solution. The spectra for the two cases agree remarkably well, verifying the close correspondence between the electronic spectral properties of the surface species and the $Rh^I(CO)_2$ moiety in the inorganic complex.

The molecular orbital energy level diagram for the square planar $Rh^ICl_2(CO)_2$ component of $[Rh^ICl(CO)_2]_2$, with C_{2v} symmetry, is shown in Figure 7A. According to Epstein et al.[25]
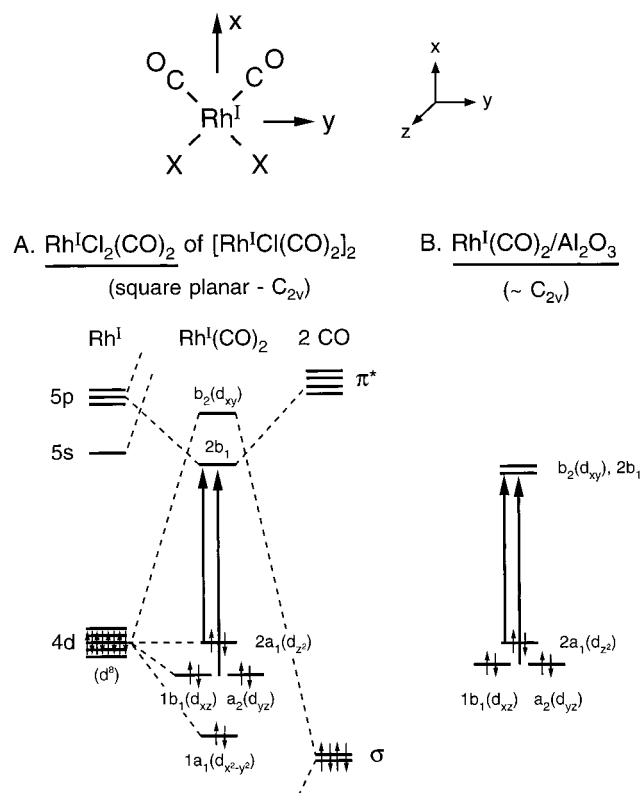

Figure 7. A.) The molecular orbital energy diagram and electronic transitions during the photoexcitation of the $Rh^I(CO)_2$ moiety of the $[Rh^ICl(CO)_2]_2$ complex. B.) The molecular orbitals involved during the electronic excitation of $Rh^I(CO)_2$/Al_2O_3 leading to Rh[I]−CO dissociation.

the absorption bands observed in the ultraviolet spectrum of $[Rh^ICl(CO)_2]_2$ can be assigned to single-electron metal-to-ligand charge-transfer excitations. The two lower energy absorption bands (3.4 and 3.9 eV) arise from the triplet and singlet components of $d_{z^2} \rightarrow L_\pi$ transitions. Specifically, the 3.9 eV feature was assigned to the spin-allowed (singlet → singlet) component of the $2a_1(d_{z^2}) \rightarrow 2b_1(L_\pi)$ transition, and the 3.4 eV feature was assigned to the spin-forbidden (singlet → triplet) component of the same transition which can take place in the presence of spin−orbit coupling when spin-multiplicity selection rules break down. The high energy band at 4.6 eV was assigned to the spin-allowed $a_2(d_{yz})$, $1b_1(d_{xz}) \rightarrow 2b_1$ transitions.

Although the excitation of an electron into the $2b_1$ molecular orbital results in a state that is antibonding in CO, the orbital is seemingly bonding in Rh−CO due to the favorable overlap of the $2\pi^*$ CO ligand with the Rh 5p orbital. Excitation to this level would not lead to efficient Rh−CO dissociation unless the excitation occurs into higher lying vibrational levels of a shallow potential energy curve for this state. Photoexcitation into the $b_2(d_{xy})$ ligand field state would, however, lead to favorable dissociation since the metal−ligand interaction in this state is antibonding in nature.[11]

The loss of a CO ligand from the ultraviolet photolysis of the $CpRh(CO)_2$ complex has been attributed to the excitation of electrons between the rhodium center d-based orbitals, or ligand-field (LF) excitations.[21] Often, a high degree of covalency is associated with the metal−ligand bond of an organometallic complex (as in the case with the back-bonding interaction between the transition metal and a CO ligand). This indicates that a fair amount of ligand character is incorporated in metal-based d → d transitions. A ligand field excitation to a higher

lying d-orbital that is also σ^* with respect to CO, will lead to rapid cleavage of the metal–ligand bond.[11,13,21] This is the case for photoexcitation into the b$_2$(d$_{xy}$) orbital for the Rh^I(CO)$_2$ surface species.

Because the precise energies of the 2b$_1$ and b$_2$(d$_{xy}$) molecular orbitals for Rh^I(CO)$_2$/Al$_2$O$_3$ are unknown, we are unable to distinguish between transitions to these levels. If the two levels were separated by a small energy difference (>0.5 eV), more features would be observed in the ultraviolet absorption spectrum due to excitations into both of these levels. The highly symmetric line shape of the 3.9 and 4.6 eV ultraviolet absorption bands indicates that the 2b$_1$ and b$_2$(d$_{xy}$) levels are relatively close in energy. Therefore, the absorption of UV light may involve excitation into either 2b$_1$ or b$_2$(d$_{xy}$) molecular orbitals as shown in Figure 7B.

The lowering of the b$_2$(d$_{xy}$) orbital energy can be rationalized by a slight deviation from perfect square planar geometry for the Rh^I(CO)$_2$/Al$_2$O$_3$ species compared to the structures of organometallic complexes. When considering square planar geometry for the surface species, it is assumed the Rh center is coordinated to two oxygen anions of the Al$_2$O$_3$ surface. The actual surface anchoring is unknown, and may in fact involve coordination of the Rh center to surface OH groups in addition to oxygen sites. This type of surface interaction has been proposed previously.[38–41] The deviation from square planar geometry will result in a lowering of the b$_2$(d$_{xy}$) level.[46] The influence of the underlying surface coordination and deviation from square planar geometry will also tend to raise the a$_2$(d$_{yz}$), 1b$_1$(d$_{xz}$) levels slightly. The slight raise will effectively lower the energy required for transitions occurring from the a$_2$(d$_{yz}$), 1b$_1$(d$_{xz}$) levels to the two unoccupied states for the Rh^I(CO)$_2$ surface species compared to the [Rh^{I}Cl(CO)$_2$]$_2$ complex. A slightly lower excitation energy was in fact observed in Figure 3.

5. Conclusions

The following conclusions have been reached concerning the ultraviolet irradiation of Rh^I(CO)$_2$/Al$_2$O$_3$ species at 205 K. (1) Surface bound Rh^{I}CO$_2$ species photodecompose into Rh^I(CO) and CO at photon energies greater than 2.8 eV. The rate of Rh^I(CO)$_2$ photodepletion is fast during initial stages of irradiation and then decreases during later stages possibly due to the slow diffusion of CO through pores of the Al$_2$O$_3$ support. (2) A lower limit of the Rh^I–CO photodissociation cross section of 3.6×10^{-20} cm^2 photon^{-1} and an initial quantum efficiency of 0.01 [Rh^I–CO dissociation] photon^{-1} has been estimated for $h\nu = 3.9 \pm 0.6$ eV from the kinetic-infrared spectroscopic analysis of the loss of Rh^I(CO)$_2$ species during photolysis. (3) The Rh^I–CO dissociation occurs from the direct electronic excitation of the Rh^I(CO)$_2$/Al$_2$O$_3$ species. (4) Spectroscopic evidence in the UV region for the formation of Rh^I(CO)$_2$ species when metallic Rh/Al$_2$O$_3$ is treated with CO has been obtained. Three absorption bands are observed at 3.3, 3.9, and 4.6 eV in the ultraviolet absorption spectra and are assigned to electronic transitions from filled Rh d-based molecular orbitals to d-based and/or ligand-based antibonding orbitals. These electronic excitations correlate well with the photon energy dependence of the photodissociation cross section of Rh^I(CO)$_2$/Al$_2$O$_3$ surface species.

References and Notes

(1) Wovchko, E. A.; Yates, J. T., Jr. *J. Am. Chem. Soc.* **1996**, *118*, 10250.

(2) Ballinger, T. H.; Yates, J. T., Jr. *J. Am. Chem. Soc.* **1992**, *114*, 10074.

(3) Ballinger, T. H.; Yates, J. T., Jr. *J. Phys. Chem.* **1992**, *96*, 9979.

(4) Wong, J. C. S.; Yates, J. T., Jr. *J. Am. Chem. Soc.* **1994**, *116*, 1610.

(5) Wong, J. C. S.; Yates, J. T., Jr. *J. Phys. Chem.* **1995**, *99*, 12640.

(6) Wovchko, E. A.; Yates, J. T., Jr. *J. Am. Chem. Soc.* **1995**, *117*, 12557.

(7) Wovchko, E. A.; Yates, J. T., Jr. *J. Am. Chem. Soc.* **1998**, *120*, 10523.

(8) Wovchko, E. A.; Yates, J. T., Jr. *J. Am. Chem. Soc.* **1998**, *120*, 7544.

(9) Wrighton, M. *Chem. Rev.* **1974**, *74*, 401.

(10) Vogler, A. In *Concepts of Inorganic Photochemistry*; Adamson, A. W., Fleischauer, P. D., Eds.; John Wiley & Sons: New York, 1975; Chapter 6.

(11) Geoffroy, G. L.; Wrighton, M. S. *Organometallic Photochemistry*; Academic Press: New York, 1979.

(12) Pourreau, D. B.; Geoffroy, G. L. In *Advances in Organometallic Chemistry*; Stone, F. G. A., West, R., Eds.; Academic Press: Orlando, 1985; Vol. 24, p 249.

(13) Lees, A. J. *Chem. Rev.* **1987**, *87*, 711.

(14) Hoyano, J. K.; Graham, W. A. G. *J. Am. Chem. Soc.* **1982**, *104*, 3723.

(15) Rest, A. J.; Whitwell, I.; Graham, W. A. G.; Hoyano, J. K.; McMaster, A. D. *J. Chem. Soc., Chem. Commun.* **1984**, 624.

(16) Rest, A. J.; Whitwell, I.; Graham, W. A. G.; Hoyano, J. K.; McMaster, A. D. *J. Chem. Soc., Dalton Trans.* **1987**, 1181.

(17) Weiller, B. H.; Wasserman, E. P.; Bergman, R. G.; Moore, C. B.; Pimentel, G. C. *J. Am. Chem. Soc.* **1989**, *111*, 8288.

(18) Belt, S. T.; Grevels, F. W.; Klotzbücher, W. E.; McCamley, A.; Perutz, R. N. *J. Am. Chem. Soc.* **1989**, *111*, 8373.

(19) Wasserman, E. P.; Moore, C. B.; Bergman, R. G. *Science* **1992**, *255*, 315.

(20) Schultz, R. H.; Bengali, A. A.; Tauber, M. J.; Weiller, B. H.; Wasserman, E. P.; Kyle, K. R.; Moore, C. B.; Bergman, R. G. *J. Am. Chem. Soc.* **1994**, *116*, 7369.

(21) Purwoko, A. A.; Drolet, D. P.; Lees, A. J. *J. Organometallic Chem.* **1995**, *504*, 107.

(22) Bromberg, S. E.; Lian, T.; Bergman, R. G.; Harris, C. B. *J. Am. Chem. Soc.* **1996**, *118*, 2069.

(23) Zubkov, T.; Wovchko, E. A.; Yates, J. T., Jr. Submitted for publication.

(24) Geoffroy, G. L.; Isci, H.; Litrenti, J.; Mason, W. R. *Inorg. Chem.* **1977**, *16*, 1950.

(25) Epstein, R. A.; Geoffroy, G. L.; Keeney, M. E.; Mason, W. R. *Inorg. Chem.* **1979**, *18*, 478.

(26) Basu, P.; Ballinger, T. H.; Yates, J. T., Jr. *Rev. Sci. Instrum.* **1988**, *59*, 1321.

(27) Wong, J. C. S.; Linsebigler, A.; Lu, G.; Fan, J.; Yates, J. T., Jr. *J. Phys. Chem.* **1995**, *99*, 335.

(28) Muha, R. J.; Gates, S. M.; Yates, J. T., Jr.; Basu, P. *Rev. Sci. Instrum.* **1985**, *56*, 613.

(29) Beebe, T. P.; Gelin, P.; Yates, J. T., Jr. *Surf. Sci.* **1984**, *148*, 526.

(30) Yates, J. T., Jr.; Duncan, T. M.; Vaughan, R. W. *J. Chem. Phys.* **1979**, *71*, 3908.

(31) Yang, A. C.; Garland, C. W. *J. Phys. Chem.* **1957**, *61*, 1504.

(32) Yates, J. T., Jr.; Duncan, T. M.; Worley, S. D.; Vaughan, R. W. *J. Chem. Phys.* **1979**, *70*, 1219.

(33) Yates, J. T., Jr.; Duncan, T. M.; Vaughan, R. W. *J. Chem. Phys.* **1979**, *71*, 3908.

(34) Rice, C. A.; Worley, S. D.; Curtis, C. W.; Guin, J. A; Tarrer, A. R. *J. Chem. Phys.* **1981**, *74*, 6487.

(35) Cavanagh, R. R.; Yates, J. T., Jr. *J. Chem. Phys.* **1981**, *74*, 4150.

(36) Yates, J. T., Jr.; Kolasinski, K. *J. Chem. Phys.* **1983**, *79*, 1026.

(37) Solymosi, F.; Pásztor, M. *J. Phys. Chem.* **1985**, *89*, 4789.

(38) van't Blik, H. F. J.; van Zon, J. B. A. D.; Huizinga, T.; Vis, J. C.; Koningsberger, D. C.; Prins, R. *J. Am. Chem. Soc.* **1985**, *107*, 3139.

(39) Robbins, J. L. *J. Phys. Chem.* **1986**, *90*, 3381.

(40) Basu, P.; Panayotov, D.; Yates, J. T., Jr. *J. Phys. Chem.* **1987**, *91*, 3133.

(41) Basu, P.; Panayotov, D.; Yates, J. T., Jr. *J. Am. Chem. Soc.* **1988**, *110*, 2074.

(42) Garland, C. W.; Wilt, J. R. *J. Chem. Phys.* **1962**, *36*, 1094.

(43) Zhou, X.-L.; Zhu, X.-Y.; White, J. M. *Surf. Sci. Rep.* **1991**, *13*, 73.

(44) Fomenko, V. S. *Handbook of Thermionic Properties*; Samsonov, G. V., ed.; Plenum Press Data Division: New York, 1966; p 37.

(45) Germer, T. A.; Ho, W. *J. Chem. Phys.* **1988**, *89*, 562.

(46) Huheey, J. E. *Inorganic Chemistry: Principles of Structure and Reactivity*, 3rd ed.; Harper & Row: New York, 1983; Chapter 11.